Structure Sensitivity of Vibrational Spectra of Mesoporous Silica SBA-15 and Pt/SBA-15

ARTICLE *in* THE JOURNAL OF PHYSICAL CHEMISTRY B · OCTOBER 2005

Impact Factor: 3.3 · DOI: 10.1021/jp051801x · Source: PubMed

6 AUTHORS, INCLUDING:

George Edward Martí
University of California, Berkeley
16 PUBLICATIONS **102** CITATIONS

SEE PROFILE

Structure Sensitivity of Vibrational Spectra of Mesoporous Silica SBA-15 and Pt/SBA-15

Yuri Borodko,[†] Joel W. Ager III,*[,†] G. Edward Marti,[†,‡] H. Song,[†] Krisztian Niesz,[†,‡] and Gabor A. Somorjai*[,†,‡]

Materials Sciences Division, Lawrence Berkeley National Laboratory, Berkeley, California 94720, and Department of Chemistry, University of California, Berkeley, California 94720

Received: April 7, 2005; In Final Form: August 1, 2005

The vibrational properties of mesoporous silica (SBA-15) were investigated by deep ultraviolet (UV) Raman and infrared spectroscopies with and without the presence of platinum nanoparticles in the mesopores that were incorporated by sonication. Raman and IR spectral line assignments were made by comparison to amorphous silicas. This procedure permitted identification of vibrations of longitudinal (LO) and transverse (TO) optical lattice modes, the presence of Si−OH, and vibrational modes associated with the presence of three-, four-, and six-membered siloxane rings. Hydraulic pressing of the mesoporous silica with pressure in the range 3−7 tons cm^{-2} destroys the X-ray diffraction pattern and strongly decreases the Raman peak (D_2) associated with three-membered rings at the surface. In the presence of platinum nanoparticles in the silica mesopores, a peak attributed to a Pt−O stretching vibration appears at between 530 and 580 cm^{-1} in the UV−Raman spectrum, which can be used to monitor the presence of the platinum particles and their interaction with the support. The D_2 feature in the UV−Raman spectra also decreases with increasing Pt loading, which is attributed to interactions of the Pt nanoparticles with the silica surface.

Introduction

Atomic-scale studies of high surface area catalyst systems present important scientific challenges that also have technological significance. In this context, mesoporous structures with long-range order, such as MCM-41[1,2] and SBA-15,[3,4] are of increasing research interest. Mesoporous structures would seem to be ideal for forming a scaffold in which a three-dimensional dispersion of metal nanoparticles could be supported, thus forming a catalyst with precise control over the location and bonding of the metal in the oxide mesopores.

Deep ultraviolet (UV) Raman spectroscopy at 244 nm can be advantageous for the study of some catalyst systems as compared to Raman spectroscopy performed in the visible range (e.g., with 488 nm excitation) due to the separation of the Raman signal from the fluorescent background.[5−10] To demonstrate the utility of the UV−Raman and Fourier transform infrared diffuse reflectance (FTIR-DRIFT) techniques, we carried out in-depth studies of mesoporous silica (SBA-15), as prepared and when compressed into a wafer, which is a common practice for catalysis studies and for the formation of industrial pelleted catalysts, and in the presence of platinum nanoparticles that were introduced by sonication into the mesopores. These studies were complemented by small-angle X-ray diffraction (SA-XRD) and transmission electron microscopy (TEM) measurements.

SBA-15 subjected to compression at high pressures has a vibrational spectrum similar to that of amorphous silicas of similar surface area. Pt loading in SBA-15 reduces the Raman scattering intensity associated with three-membered siloxane rings at the surface. The presence of platinum nanoparticles in the mesopores could be identified by the appearance of a low-frequency Pt−O vibrational mode between 520 and 580 cm^{-1}. This mode shifts to lower frequency with increasing Pt loading, suggesting an increase in the interaction of the Pt nanoparticles with the oxide support.

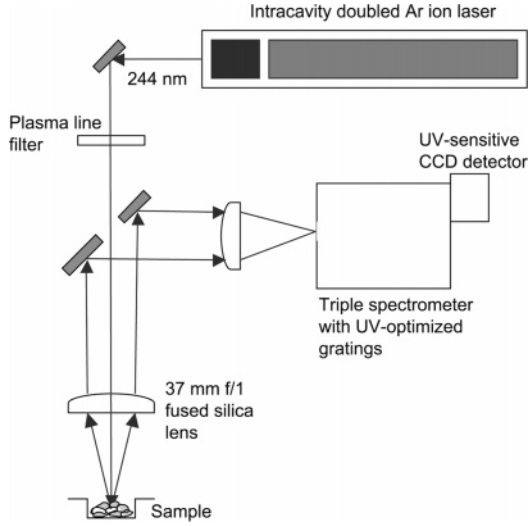

Figure 1. Overview of UV−Raman spectroscopy system.

The deep-UV Raman spectroscopy system has been described in detail before.[9] A summary will be given here and an overview of the setup is shown in Figure 1. A continuous wave (cw), intracavity-doubled, argon ion laser operating at 244 nm is used as the excitation source, and a custom designed (Omega Optical) UV long-pass edge filter is used to block plasma lines below 246 nm. The laser is focused to a ∼500 μm spot on the surface of the catalyst by a 37 mm f/1 fused silica lens. Backscattered light is collected with the same lens, collimated, and directed to the entrance slit of a triple spectrometer optimized for performance in the deep-UV regime. Some spectra were taken with an additional band-pass filter in front of the spectrometer

* To whom correspondence should be addressed: E-mail: JWAger@lbl.gov (J.W.A.), GASomorjai@lbl.gov (G.A.S.).
[†] Lawrence Berkeley National Laboratory.
[‡] University of California.

10.1021/jp051801x CCC: $30.25
Published on Web 08/26/2005

to further reduce the intensity of elastic scattering. Spectra were recorded with a LN-cooled, UV-enhanced CCD camera. The instrument dispersion is 2.1 cm^{-1}/pixel; the typical resolution used was 12 cm^{-1} and was controlled by the slit width of the dispersion stage of the triple spectrometer. Typical collection times were 10−30 min using 3−5 mW of 244-nm excitation. Hexagonal BN powder was added to the SBA-15 samples as an internal intensity reference.

FTIR-DRIFT spectra were measured with Nicolet Nexus-670 spectrophotometer with integrated diffuse reflectance optics (Spectra-Tech Collector II). We found that for the materials studied here, somewhat better spectra could be obtained by using a 30−50 μm thick powder layer on a reflective surface such as gold in place of the standard DRIFT sample holder. As the layer thickness can be adjusted to be partly IR transparent, we could optimize the ratio of diffuse reflectance to specular reflectance, obtaining spectra similar to those measured in transmission. The method is best described as a hybrid of DRIFT and IR reflection absorption spectroscopy (IRRAS).

SBA-15 was made using the standard procedure.[3] Pluronic P123 (BASF, $EO_{20}PO_{70}EO_{20}$, EO = ethylene oxide, PO = propylene oxide) and tetraethoxysilane (TEOS, 99+%, Alfa Aesar) were used as received. Pluronic P123 (6 g) was dissolved in 45 g of water and 180 g of 2 M HCl solution with stirring at 35 °C for 30 min. TEOS (12.75 g) was added to the solution with stirring at 35 °C for 20 h. The mixture was aged at 373 K for 24 h. The white powder was recovered through filtration, washed with water and ethanol thoroughly, and dried in air. The product was calcined at 550 °C for 12 h in air.

Our group and others have been developing methods to achieve metal particle incorporation into mesoporous structures.[11−14] Our synthetic procedure for Pt nanoparticles has been described in detail previously;[14] a summary will be given here. Platinum particles with 2.9-nm average diameter were synthesized by an alcohol reduction technique using poly(vinylpyrrolidone) (PVP) to stabilize the particles by capping them in aqueous media.[15,16] PVP (133 mg, M_w = 29 000) was dissolved in a mixture of 180 mL of methanol and 20 mL of 6 mM hexachloroplatinic acid ($H_2PtCl_6 \cdot 6H_2O$) aqueous solution. The mixture was heated to reflux temperature and stirred for 3 h to complete the reduction. Then the solvent was evaporated, and the particles were redispersed in water adjusting the concentration of the final solution to 3 mM. The appropriate amount of Pt particles in water/ethanol mixture (1:1) was incorporated into the SBA-15 silica mesostructure by mechanical force using low-power sonication for 3 h (70 W, 42 kHz). After centrifuging, the brown residue was washed with water and ethanol and dried at 80 °C under air overnight. To remove carbonaceous species from the surface of the particles, the Pt/SBA-15 catalyst was calcined at 450 °C for 12 h in flowing oxygen. Amorphous fumed silica (Cab-O-Sil, surface area 250 m^2/g), silica gel (Davidson grade 57, surface area 220 m^2/g, 60−100 mesh), a commercial 2% Pt on Al_2O_3 dispersed metal catalyst (Exxon reforming catalyst HFR-100), and Pt powder (Alfa Aesar, 99.9% Pt, surface area 9.2−15.7 m^2/g, 0.10−0.25 μm particle size) as received from the manufacturers were used as a comparison standards.

A number of other standard characterization methods were employed to study SBA-15 with and without Pt nanoparticles. Small-angle X-ray scattering measurements were performed with a Bruker Nanostar U instrument using Cu Kα radiation (1.54 Å) and a 107-cm sample to detector distance. TEM studies were performed on a Topcon EM002B microscope. A TEM micrograph of a typical Pt/SBA-15 sample is shown in Figure 2.

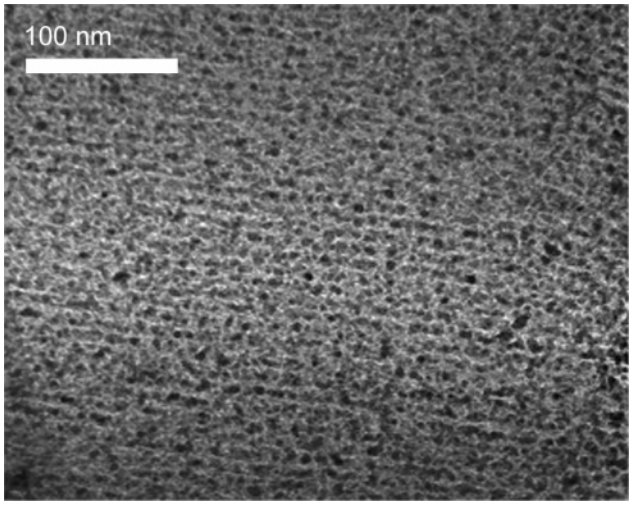

Figure 2. TEM image of 14 wt % Pt/SBA-15 catalyst made by the capillary inclusion (CI) method. It has a surface area of 800 $m^2\ g^{-1}$ and pore size of 9 nm.

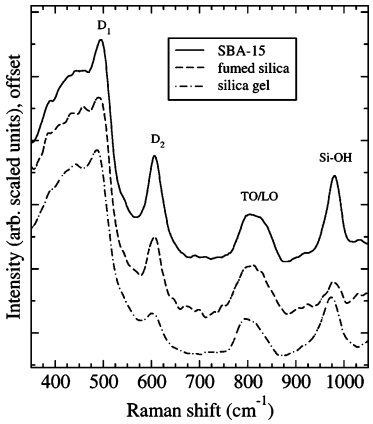

Figure 3. UV−Raman spectrum (244 nm excitation) of as-calcined SBA-15 (surface area = 765 $m^2\ g^{-1}$) and two amorphous silicas with surface areas of about 200 $m^2\ g^{-1}$. The broad feature near 430 cm^{-1} is assigned to six-membered rings in the network and the D_1 and D_2 features at 492 and 606 cm^{-1} are assigned to vibrationally isolated four- and three-membered siloxane rings. The broad feature near 810 cm^{-1} is assigned to overlapping TO and LO modes of network motions The peak at 960 cm^{-1} is attributed to free surface silanols.

Nitrogen porosity measurements were performed using a Quantachrome Autosorb-1 at 77 K. After calcination at 550 °C, the SBA-15 had a pore diameter of 9 nm and a surface area of 765 $m^2\ g^{-1}$. We have shown elsewhere that for Pt/SBA-15 made with the sonication method, the nanoparticles are in the channels, do not block them, and are catalytically active.[14]

Results and Discussion

Figure 3 shows the UV−Raman spectrum of SBA-15 without Pt in the 350−1050 cm^{-1} range. The spectra of two amorphous silicas are shown for comparison. The UV−Raman spectra resemble those of published visible Raman spectra of amorphous silicas and silica glasses. The visible Raman spectrum of SiO_2 has been studied extensively; we use here assignments developed by Galeneer et al.[17,18] and discussed in the review of Sharma et al.[19] The assignments are summarized in Table 1. The broad feature near 430 cm^{-1} is assigned to six-membered rings in the network, and the D_1 and D_2 features at 492 and 606 cm^{-1} are assigned to symmetric O−Si−O motions of vibrationally isolated (i.e. localized) four-membered rings of SiO_4 tetrahedra and to breathing motions of three-membered rings of SiO_4

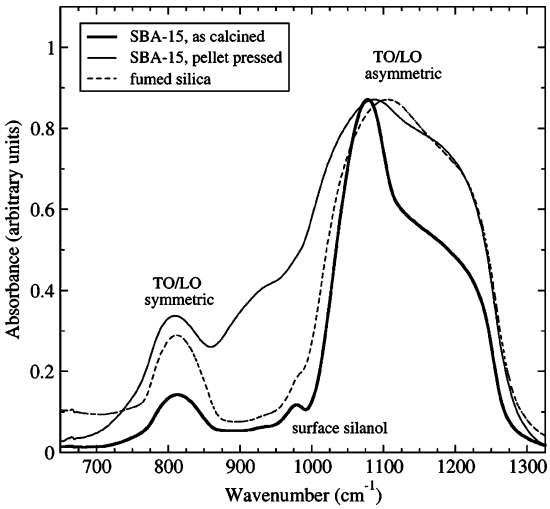

Figure 4. FTIR-DRIFT spectra of as-calcined SBA-15 and amorphous fumed silica (Cab-O-Sil). The spectrum of SBA-15 subjected to pellet pressing at 7 tons cm^{-2} is also shown. The band centered at 810 cm^{-1} and the bands at 1100 and 1180 cm^{-1} are assigned to symmetric and asymmetric TO/LO lattice modes, respectively. The band at 980 cm^{-1} in SBA-15 is assigned to surface silanol groups.

TABLE 1: Assignments of UV−Raman (UV−R) and IR Spectral Features for SBA-15 and Pt/SBA-15

peak position (cm^{-1})	observed	assignment
430, br	UV−R	six-membered rings in silica network
492	UV−R	D_1, localized four-membered siloxane rings
606	UV−R	D_2, localized three-membered siloxane rings
810	UV−R, IR	symmetric TO/LO, splitting not resolved
960	UV−R, IR	Si-OH
1110, 1180	UV−R, IR	asymmetric TO/LO

tetrahedra, respectively.[20] The combined feature at 800 and 830 cm^{-1} is assigned to the transverse (TO) and longitudinal (LO) optical components, respectively, of network motions. We attribute the band at 960 cm^{-1} to the Si−OH stretching of free surface silanols.[21] Compared to both amorphous silicas, the D_2 peak is relatively stronger in SBA-15. The three membered $(SiO)_3$ rings thought to be responsible for D_2 are also thought to be preferentially formed at surfaces; D_2 is observed to be stronger, in general, in higher surface area material.[22] Thus, here we attribute the strong D_2 and silanol peaks in SBA-15 to its higher surface area compared to the standard silicas measured.

Figure 4 shows the FTIR-DRIFT spectrum of as-calcined SBA-15 and amorphous silica. As with the UV−Raman spectrum, features are similar to those of amorphous SiO_2. The band centered at 810 cm^{-1} is assigned to symmetric LO and TO lattice modes. The bands at 1100 and 1180 cm^{-1} are assigned to asymmetric TO and LO lattice modes. The band at 980 cm^{-1} is assigned to surface silanol modes. The surface silanol feature is stronger and the 1180 cm^{-1} asymmetric LO feature is weaker in SBA-15 as compared to amorphous silica. The stronger silanol peak is consistent with the UV−Raman data and is attributed to the higher surface area of SBA-15.

Compared to other mesoporous materials such as MCM-41, SBA-15 has larger pores and an unfavorable ratio of wall-thickness to unit cell size, leading to mechanical instability. The standard technique of pellet pressing (pressures in the range of 3−7 tons cm^{-2}) used to make samples for transmission FTIR studies causes the collapse of the mesoporous structure, as seen in the diffraction patterns shown in Figure 5; a similar effect was reported earlier by Hartman and Vinu[23] for SBA-15

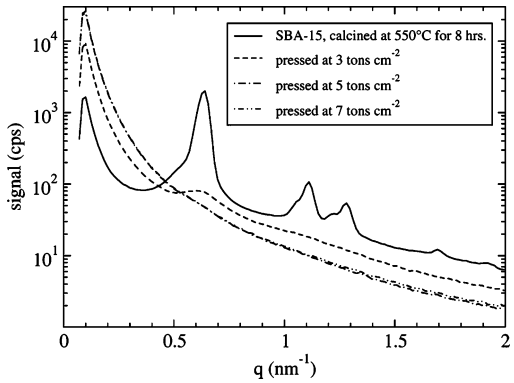

Figure 5. Small-angle XRD patterns of as-calcined SBA-15 subjected to hydraulic pellet pressing at pressures between 3 and 7 tons cm^{-2} for 3 min.

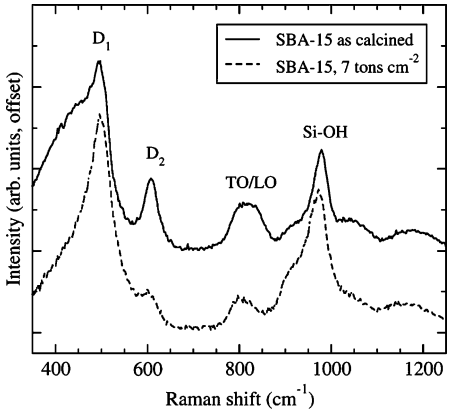

Figure 6. UV−Raman spectra of as-calcined SBA-15 (765 m^2/g) and SBA-15 subjected to hydraulic pellet pressing at 7 tons cm^{-2} for 3 min (265 m^2/g). The D_2 feature (three-membered siloxane rings associated with the surface) is weaker and the Si−OH feature is stronger after pellet pressing.

subjected to pressures in the 0.6−2.9 tons cm^{-2} range. Subsequent porosimetry revealed a drop in the surface area from 765 to 265 $m^2\ g^{-1}$ and a smaller, bimodal pore size distribution peaked at 2.4 and 3.7 nm for the highest pressure used (Supporting Information, Figure S1).

FTIR-DRIFT and UV−Raman and spectra of as-grown and pressed SBA-15 are shown in Figures 4 and 6. Collapse of the mesoporous structure produces observable changes in both spectra. In the UV−Raman spectrum (Figure 6) pressing causes a decrease in D_2; this is consistent with the decreased surface area. Also, the intensity near 430 cm^{-1} decreases, while the D_1 feature retains its intensity. This is roughly consistent with work that shows that application of much higher stresses (up to 4 GPa) in silica optical fibers causes a decrease of the peak intensity at 440 cm^{-1}, while the D_1 peak at 490 cm^{-1} remains unchanged.[24] The most prominent changes in the DRIFT spectra (Figure 4) due to pressing are a broadening of all of the bands and a relative increase of the feature at 1180 cm^{-1}. The overall result is that the SBA-15 spectrum becomes more like that of amorphous silica of similar surface area.

A key challenge in using SBA-15 as a catalytic material is introducing metal into its channels in such a way that preserves their structure. In this context, we found recently that when SBA-15 was grown in the presence of metal nanoparticles, the final pore lattice parameter in SBA-15 could be increased by as much as 10%.[25] Small-angle XRD patterns of SBA-15 with 2.9 nm Pt nanoparticles loadings up to 7.3 wt. % are shown in Figure 7. The mesoscopic order is clearly preserved at the highest Pt loading, although there is a small decrease in the

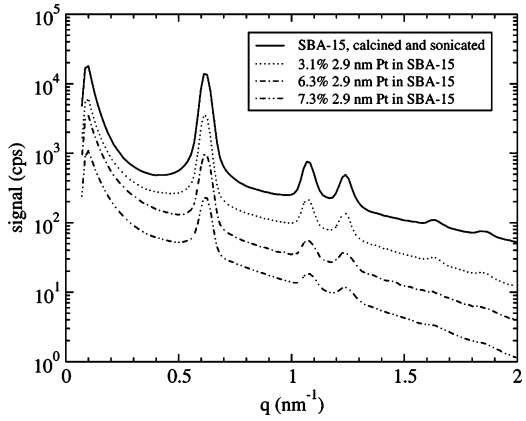

Figure 7. Small-angle XRD patterns of SBA-15 loaded with 2.9-nm diameter Pt nanoparticles up to 7.3 wt %. Spectra are offset for clarity.

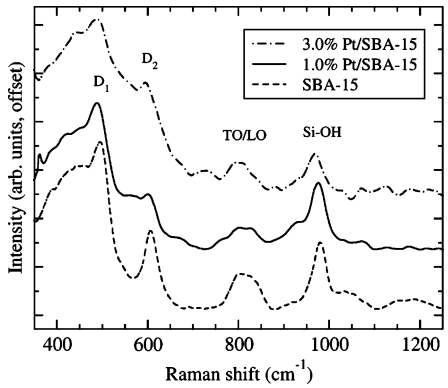

Figure 8. UV−Raman spectra of SBA-15 as a function of Pt loading at low Pt loading. The D_2 feature associated with the three-membered siloxane rings decreases with increasing Pt loading. The increasing background between 400 and 600 cm^{-1} in the 3% Pt/SBA-15 spectrum is attributed to the Pt−O stretch (see Figure 9).

relative intensities of the higher order reflections [(210) and (300)] in the samples with 6.3 and 7.3% loading.

UV−Raman and FTIR-DRIFT were employed to characterize in more detail changes to the structure of SBA-15 as a function of metal loading. Raman spectra of Pt/SBA-15 as a function of Pt loading are shown in Figure 8. The D_2 peak at 605 cm^{-1} clearly decreases with Pt loading, while the silanol peak decreases, but to a lesser degree. We also obtained spectra (not shown) from SBA-15 that was sonicated in the absence of Pt nanoparticles. In these spectra, there is only a slight decrease in the height of the D_2 peak compared to that of SBA-15 sonicated with Pt. Thus, we can attribute the decrease of the D_2 peak to a decrease in the concentration of reactive three-membered Si−O rings at the surface caused primarily by the incorporation of Pt nanoparticles.

In Figure 8, the background appears to increase in the vicinity of 550 cm^{-1} in the Raman spectrum of the 3.0% Pt/SBA-15. At higher Pt loadings, a broad peak centered between 530 and 580 cm^{-1} becomes prominent and the SiO_2 Raman features cannot be distinctly observed. Figure 9 shows difference spectra for Pt/SBA-15 (3% and 7% loading) and for two commercial supported Pt catalysts. In general, metal particles are not directly observable by vibrational spectroscopy. However, the signal from the surface metal oxide can be strong in UV−Raman. For example, consistent with previous UV−Raman studies of dispersed Pt/Al_2O_3,[10] we find that the PtO stretch is the dominant feature in Pt/SBA-15 at higher metal loadings. More specifically, Uy et al.[10] observed the Pt−O feature at 571 cm^{-1} in Pt/γ-Al_2O_3, assigned it to the Pt−O stretch, and attributed it to the

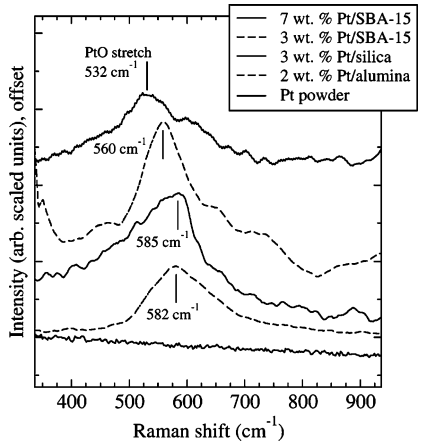

Figure 9. Comparison of UV−Raman spectra in the Pt−O stretch region for SBA-15 with two loadings of Pt nanoparticles, 3 wt % Pt dispersed on amorphous silica and 2 wt % Pt dispersed on alumina. The data are obtained by subtracting the spectrum of the unloaded support in each case. The position of the PtO_x stretch feature is indicated.

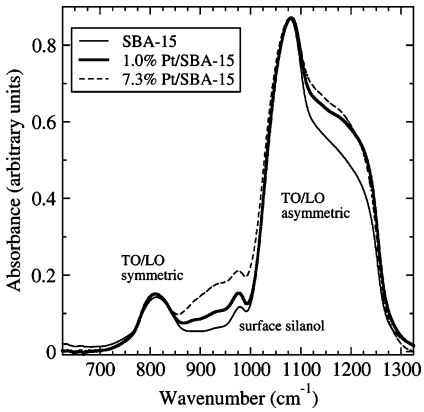

Figure 10. FTIR-DRIFT spectra of SBA-15 as a function of 2.9-nm Pt nanoparticle loading. The relative intensity of the LO phonon at 1180 cm^{-1} increases with Pt loading in SBA-15.

presence of atomic O at step and terraces on the Pt. Here, we observed that the peak appears at lower frequency for Pt/SBA-15 as compared to Pt/silica. In addition, the peak shifts to lower frequency in SBA-15 with increasing loading. It is possible that this is due to changes in the Pt-support interaction as the loading is increased in SBA-15. We note that dispersed Pt powder did not exhibit the PtO stretch feature. It may be that because the average particle size (170 nm) is much larger than for the particles in Pt/SBA-15, the amount of PtO is too small to detect. Figure S2 in the Supporting Information shows UV reflectance data from Al_2O_3 and Pt-loaded Al_2O_3. It can be seen that Pt-loading increases the sample absorption, and that the effect is particularly strong in the spectral region near 244 nm. We consider it possible that observation of the PtO surface vibrations in Pt-loaded Al_2O_3 and SBA-15 is enhanced by a UV−Raman resonance process. It is unlikely that there is a SERS-like enhancement process due to the expected strong damping of the Pt surface plasmon modes at the laser frequency used.

Figure 10 shows the FTIR-DRIFT spectra as a function of Pt loading in SBA-15. The relative intensity of the LO phonon at 1180 cm^{-1} increases with Pt loading. Again, this is similar, but smaller in magnitude, to the effect seen with pellet pressing. This might be consistent with the small change in mesoscopic order found with increasing Pt loading in the XRD data shown in Figure 7.

Conclusions

Vibrational spectroscopy, specifically deep UV−Raman and FTIR-DRIFT, are shown to be useful for assessing changes in the internal structure of mesoporous silica-based SBA-15. By using external hydraulic pressure to destroy the mesoscopic order without changing the chemical composition, the UV−Raman and IR bands specifically associated with mesoscopic order could be assigned. It is shown that vibrations associated with three-membered −Si−O− rings (D_2 Raman feature), surface silanol (980 cm^{-1}, Raman and IR), and the asymmetric component of the Si−O−Si LO phonon (IR, 1180 cm^{-1}) are particularly sensitive. In metal-loaded SBA-15 made by sonication with Pt nanoparticles, it is shown that with increasing Pt loading, changes are observed in both UV Raman and FTIR spectra. The strongest effect is a decrease in the concentration of three-membered siloxane rings with increasing Pt loading. In addition, the position of the PtO stretching vibration observed in UV−Raman may be used to probe the strength of the interactions of the metal nanoparticles with the oxide support.

Acknowledgment. This work was supported by the Director, Office of Science, Office of Basic Energy Sciences, Division of Chemical Sciences, of the U.S. Department of Energy under Contract No. DE-AC03-76SF00098. We thank Prof. E. Iglesias and B. Model for the use of their UV reflectance instrumentation. Use of the National Center for Electron Microscopy for the TEM studies is acknowledged. K.Z. was supported by the National Science Foundation under contract DMR-0244146. H.S. thanks the Korea Science and Engineering Foundation (KOSEF) for support under the Postdoctoral Fellowship Program.

Supporting Information Available: Figures showing nitrogen porosity measurements on SBA-15 before and after pellet pressing and UV−visible diffuse reflectance spectra of Al_2O_3 and 2% Pt/Al_2O_3. This material is available free of charge via the Internet at http://pubs.acs.org.

References and Notes

(1) Kresge, C. T.; Leionowicz, M. E.; Roth, W. J.; Vartuli, J. C.; Beck, J. S. *Nature* **1992**, *359*, 710.
(2) Beck, J. S.; Vartuli, J. C.; Roth, W. J.; Leonwicz, M. E.; Kresge, C. T.; Schmitt, K. D.; Chu, C. T.-W.; Olson, D. H.; Sheppard, E. W.; McCullen, S. B.; Higgins, J. B.; Schlenker, J. L. *J. Am. Chem. Soc.* **1992**, *114*, 10834.
(3) Zhao, D.; Yang, P.; Melosh, N.; Feng, J.; Chmelka, B. F.; Stucky, G. D. *Adv. Mater.* **1998**, *10*, 1380.
(4) Zhao, D.; Huo, Q.; Feng, J.; Chmelka, B. F.; Stucky, G. D. *J. Am. Chem. Soc*. **1998**, *120*, 6024.
(5) Stair, P. C.; Li, C. *J. Vac. Sci. Technol. A* **1997**, *15*, 1679 and references therein.
(6) Xiong, G.; Feng, Z.; Li, J.; Yang, Q.; Ying, P.; Xin, Q.; Li, C. *J. Phys. Chem. B* **2000**, *104*, 3581.
(7) Rzhevskii, A. M.; Choi, P.; Ribeiro, F. H.; Gulotty, R. J., Jr.; Olken, M. M. *Catal. Lett.* **2001**, *73*, 187.
(8) Chua, V. T.; Stair, P. C.; Wachs, I. E. *J. Phys. Chem. B* **2001**, *105*, 8600.
(9) Tewell, C. R.; Malizia, F.; Ager, J. W., III; Somorjai G. A. *J. Phys. Chem B* **2002**, *106*, 2946.
(10) Uy, D.; O'Neill, A. E.; Weber, W. H. *Appl. Catal. B: Environ.* **2002**, *35*, 219.
(11) Han, Y.-J.; Kim, J. M.; Stucky, G. D. *Chem. Mater.* **2000**, *12*, 2068.
(12) Kónya, Z.; Puntes, V. F.; Kiricsi, I.; Zhu, J.; Ager, J. W., III; Ko, M. K.; Frei, H.; Alivisatos, A. P.; Somorjai, G. A. *Chem. Mater.* **2003**, *15*, 1242.
(13) Zhu, J.; Kónya, Z.; Puntes, V. F.; Kiricsi, I.; Miao, C. X.; Ager, J. W., III; Alivisatos, A. P.; Somorjai, G. A. *Langmuir* **2003**, *19*, 4396.
(14) Rioux, R. M.; Song, H.; Hoefelmeyer, J. D.; Yang, P.; Somorjai, G. A. *J. Phys. Chem. B.* **2005**, *109* (6), 2192−2202.
(15) Teranishi, T.; Hosoe, M.; Tanaka, T.; Miayke, M. *J. Phys. Chem B* **1999**, *103*, 3818.
(16) Wang, Y.; Ren, J.; Deng, K.; Gui, L.; Tang, Y. *Chem. Mater.* **2000**, *12*, 1622.
(17) Galeener, F. L.; Lucovsky, G.; *Phys. Rev. Lett.* **1976**, *37*, 1474.
(18) Geissberger, A. E.; Galeener, F. L. *Phys. Rev. B* **1983** *28*, 3266.
(19) Sharma, S. K.; Cooney, T. F.; Wang, Z.; van der Laan, S. *J. Raman Spectrosc.* **1997**, *28*, 697.
(20) Rahmani, A.; Benoit, M.; Benoit, C. *Phys. Rev. B* **2003**, *68*, 184202.
(21) Morrow, B. A.; McFarlan, A. J. *J. Non-Crys. Solids* **1990**, *120*, 61.
(22) Brinker, C. J.; Kirkpatrick, R. J.; Tallant, D. R.; Bunker, B. C.; Montez, B. *J. Non-Cryst. Solids* **1988**, *99*, 418.
(23) Hartman, M.; Vinu, A. *Langmuir* **2002**, *18*, 8010.
(24) Hibino, Y.; Hanafusa, H.; Ema, K.; Hyodo, S.-I. *Appl. Phys. Lett.* **1985**, *47*, 812.
(25) Kónya, Z.; Puntes, V. F.; Kiricsi, I.; Zhu, J.; Alivisatos, A. P.; Somorjai, G. A. *Nano Lett.* **2002**, *2*, 907.